Journal of Applied Electrochemistry **29**: 987–994, 1999.

Study of pyrite oxidation by cyclic voltammetric, impedance spectroscopic and potential step techniques

H.K. LIN[1] and W.C. SAY[2]
[1]*Mineral Industry Research Laboratory, University of Alaska Fairbanks, Fairbanks, Alaska 99775-7240;*
[2]*Department of Materials Science, National Taipei Institute of Technology, Taipei, Taiwan*

Received 21 August 1998; accepted in revised form 18 January 1999

Key words: cyclic voltammetry, impedance spectroscopy, potential step chronoamperometry, pyrite

Abstract

Pyrite oxidation in chloride solutions was investigated with cyclic voltammetry, a.c. impedance and potential step techniques. The oxidation reactions of pyrite were examined by cyclic voltammetric technique and a two-step reaction with a passivation film forming as a first-step product was proposed. An equivalent circuit was then postulated based on the oxidation reactions. Parameters indicated in the equivalent circuit such as reaction resistance and pseudo-capacitance caused by the passivation film, were determined by a.c. impedance measurements. A mathematical formula was derived from the concept of the equivalent circuit to explain the depression of the semicircle in the complex plane plot. When the semicircle is depressed, the mathematical formula indicates that the reaction resistance should be obtained from the intersection of the semi-circle with Z'-axis instead of the semicircle diameter. Potential step chronoamperometric technique was then applied to measure the charging current, which is caused by the pseudo-capacitance of the passivation film, to examine the proposed equivalent circuit. The peak charging current densities at 1.10 and 0.90 V vs SHE obtained from the equivalent circuit and the a.c. impedance measurements are 110 and 75 mA cm^{-2}, respectively. They are consistent with the peak current densities of 105 and 69 mA cm^{-2} at 1.10 and 0.90 V, respectively, determined by the potential step chronoamperometric measurements.

1. Introduction

Pyrite is the most abundant sulfide mineral; it is very common in coals, hydrothermal veins, contact metamorphic deposits and sedimentary rocks. It is frequently associated with valuable sulfide minerals, gold, and coal; thus, it has been the subject of extensive research in view of coal processing, extractive metallurgy as well as acid mine drainage [1–6]. The pyrite-bearing coals emit sulfur dioxide when combusted and the emission causes environmental concerns. When pyrite in mines or wastes is oxidized, acid mine drainage is produced and has to be treated. Pyrite also interferes with gold and base metal extraction processes. The kinetic data obtained in this study may be used to estimate the pyrite oxidation rate and hence to assist pyrite removal processes in coal processing, extractive metallurgy and acid mine drainage treatments.

Electrochemical measurements, cyclic voltammetry in particular, have been employed to study the oxidation of pyrite. The measurements were obtained mainly to study oxidation reactions and reaction mechanisms. In the oxidation of pyrite, SO_4^{2-}, $Fe(OH)_3$ and Fe^{3+} were suggested as the reaction products with elemental sulfur as an intermediate [6–10]. Recently, Li et al. confirmed the formation of elemental sulfur and polysulfide over a wide range of pH using *in situ* Raman spectroscopy [11].

Impedance measurements of electrochemical processes have been widely adopted in the study of corrosion engineering since the early 1980s. The technique was employed in corrosion engineering, mainly to investigate corrosion kinetics and to predict corrosion rates [12–13]. More recently, this technique has been applied to mineral dissolution processes [14–15]. The reported complex plane plots at various electrolytes were depressed with an angle along the Z'-axis. The depression was also observed in this study and the effect of the depression on the determination of the kinetic parameters is discussed.

In the present study, oxidation reactions are postulated based on cyclic voltammetry. The electrochemical characteristics of the reactions are also examined by analysing the data obtained by cyclic voltammetry. An equivalent circuit is postulated based on the oxidation reactions. Related kinetic parameters, as indicated in the equivalent circuit, are determined by a.c. impedance measurements. The equivalent circuit and some parameters are then examined by a potential step chronoamperometry.

2. Experimental details

A pyrite sample with relatively high purity, originating from Custer, South Dakota, was obtained from Ward's Natural Science Establishment, Inc. Pyrite cylinders were prepared from the pyrite sample to make working electrodes. The surface area of the pyrite electrode exposed to the electrolyte was 14.3 mm^2. The procedure for preparing the working electrode is described elsewhere [17]. The working electrode was pretreated by polishing with 0.05 μm aluminium powder and washed with distilled water. Microscopic examinations of the electrode revealed that a trace amount of quartz might occasionally appear in the electrode. Chemical analysis indicated that a trace amount of copper and nickel exist. Immediately before starting each test, the electrode was pretreated again.

An H-type three-electrode cell with a sintered Pyrex disc of fine porosity was provided by EG&G Princeton Applied Research. A platinum electrode and a saturated calomel electrode served as the auxiliary and the reference electrodes, respectively. The electrolyte in the cell was thermostated in a water bath and was controlled by a J-KEM temperature controller. An EG&G potentiostat (model 273A) and a lock-in amplifier (EG&G, model 5210) were employed for the electrochemical measurements. A PS/2 computer was used to command the tests. The schematic diagram of the set-up is given elsewhere [16].

Ultra-high purity nitrogen was used for purging the electrolyte for 30 min before each test and as a shielding atmosphere in the cell during the tests. The electrolyte contained 4.5 M NaCl and 0.5 M HCl unless otherwise stated. Sodium chloride and hydrochloric acid were of analytical grade. The electrolyte temperature was maintained at 25 °C for all tests.

The solution ohmic drop was compensated by the positive feedback method in the electrochemical measurements. Potentials were reported with respect to the standard hydrogen electrode (SHE) unless otherwise stated.

3. Results and discussion

3.1. *Cyclic voltammetry*

The objects of the cyclic voltammetric study are to postulate the related oxidation reactions and to characterize the nature of the reactions.

Cyclic voltammetry tests were conducted in quiescent electrolytes at various scan rates. A typical cyclic voltammogram of the pyrite oxidation in this study is given in Figure 1. Three cycles were scanned for each voltammetric test and the third cycle was reported as the cyclic voltammogram. In the cyclic voltammetric tests, the potential was scanned from 0.10 V (vs SHE) to 1.20 V and back to 0.10 V. The peak current density, i_p, at the peak potential E_p appears in the cyclic voltammogram. E_p varied from 0.75 to 0.95 V vs SHE depending on the scan rate. A similar peak was observed in this potential range for pyrite oxidation in a weak alkaline solution and was attributed to the formation of ferric hydroxide or a sulfur film [7, 8]. The proposed reaction is

$$FeS_2 + 3\,H_2O = Fe(OH)_3 + 2\,S^0 + 3\,H^+ + 3\,e^- \qquad (1)$$

Due to the high acidity of the electrolyte (0.5 M HCl) in the present research, a ferric hydroxide film is unlikely. A sulfur film or polysulfides, products of the first-step reaction, thus caused the appearance of the peak. The sulfur and the polysulfides were then further oxidized to sulfate at a higher potential. Sulfate was the predominant final product. The sulfur film was chosen to represented the first-step reaction and the simplified anodic reactions can be written as

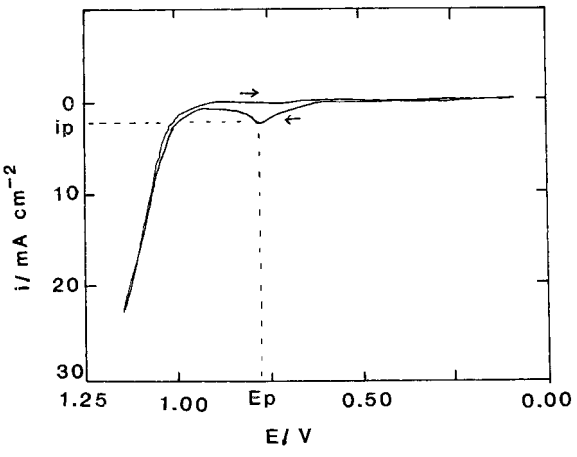

Fig. 1. Voltammogram of pyrite oxidation at 20 mV s^{-1}.

First-step

$$FeS_2 = Fe^{2+} + 2S^0 + 2e^- \quad (2)$$

Second-step

$$S^0 + 4H_2O = SO_4^{2-} + 8H^+ + 6e^- \quad (3)$$

Obviously, Reaction 3 is a simplified reaction and intermediate products exist before sulfate is produced. The sulfur film was very thin; an examination of the reacted electrode by a microprobe technique failed to identify the presence of the film. However, the existence of sulfur has been confirmed in a similar system using *in situ* Raman spectroscopy [11]. The thickness of the film is a characteristic of the dynamic equilibrium between Reactions 2 and 3; thus, it is a function of the applied potential. At a higher potential, the oxidation of sulfur to sulfate (Reaction 3) is faster. On the other hand, the production of sulfur (Reaction 2) is also faster at a higher potential, especially when part of the sulfur film is rapidly oxidized at high potentials.

Both i_p and E_p were found to be a function of the scan rate, v. A plot of i_p against $v^{1/2}$ shows a linear relationship, as indicated in Figure 2. Thus the reaction corresponding to the peak is controlled by diffusion and the mathematical formulation of this linear relation has been given elsewhere [17]. The current drop at E_p is considered to be due to the passivation of the sulfur film. The diffusion of either electrons or ferric ions is thus retarded. As shown in Figure 3, a linear relationship was also observed in a plot of E_p against the logarithm of scan rate (log v). The linear relationship indicates that the reaction is irreversible [17].

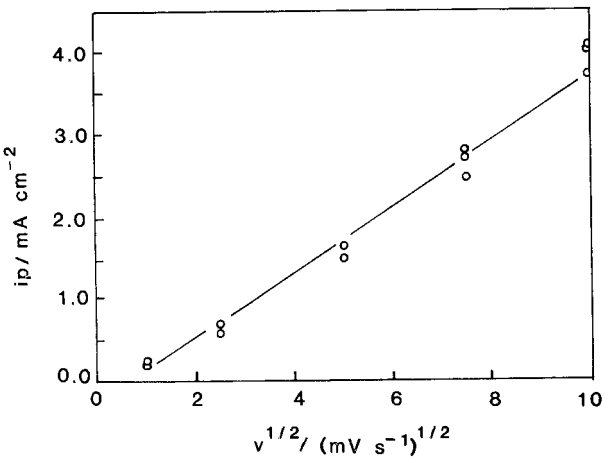

Fig. 2. Linear relationship between peak current density and square root of the scan rate.

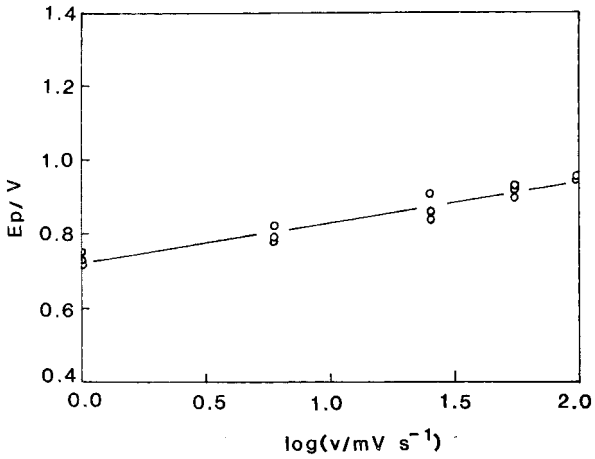

Fig. 3. Linear relationship between peak potential and logarithm of the scan rate.

In separate tests, rotating speeds of 200 and 500 rpm were applied to the working electrode using the rotating disc technique. No difference in the magnitude of i_p was observed between the two rotation speeds at 1.10 V. Thus, the diffusion is unlikely to be external diffusion; rather, it is diffusion through a passive film. This is consistent with the proposed oxidation reactions.

3.2. *Impedance measurements*

Where the data obtained in the cyclic voltammetry study was used to propose the related reactions, the a.c. impedance spectroscopy was applied to determine the kinetic parameters in the corresponding equivalent circuit.

Alternating current impedance measurements were performed at 0.9 and 1.1 V vs SHE with frequencies ranging from 5 to 10^5 Hz. The a.c. amplitude was 5 mV. The complex plane plots (Nyquist plots) of the a.c. impedance measurements are given in Figures 4 and 5, where Z' and Z'' are real and imaginary parts of the impedance, respectively.

Based on the proposed oxidation reactions, an equivalent circuit of the overall reaction was postulated. The equivalent circuit is shown in Figure 6, where R_s is the solution resistance; R_1 and R_2 are the resistance of Reactions 2 and 3, respectively; C_p is the pseudo-capacitance of the film; and C_d is the double-layer capacitance on the electrode-solution interface.

The solution resistance was compensated by the positive feedback method and C_d was insignificant as compared to C_p [16]. In both Figures 4 and 5, the semicircle of the complex plane plot is depressed at an angle α against the Z'-axis. It has been suggested that the depression is caused by the uneven distribu-

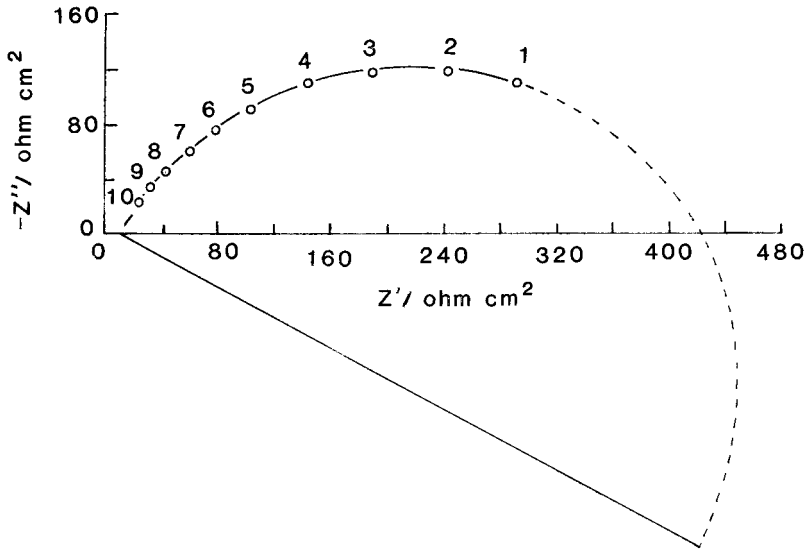

Fig. 4. Complex plane plot with a.c. amplitude of 5 mV at 1.10 V vs SHE in the frequency range of 5 to 10^5 Hz.

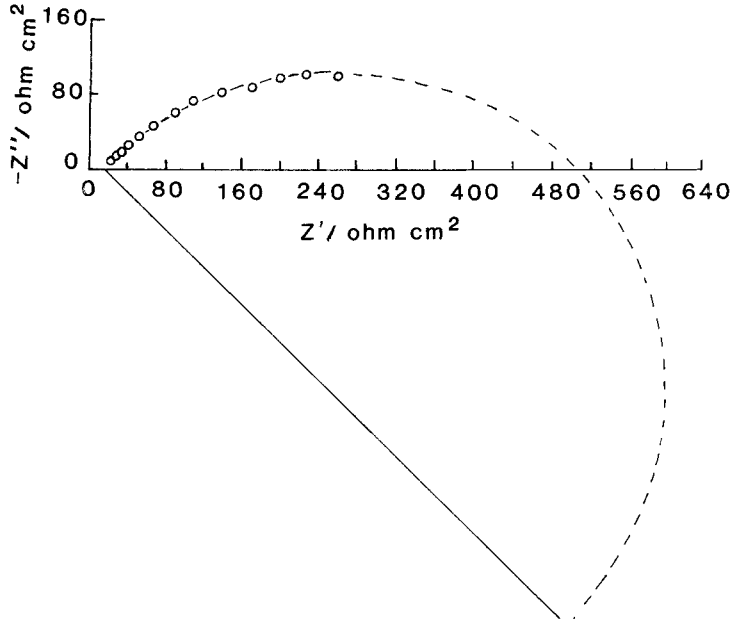

Fig. 5. Complex plane plot with a.c. amplitude of 5 mV at 0.90 vs SHE in the frequency range of 5 to 10^5 Hz.

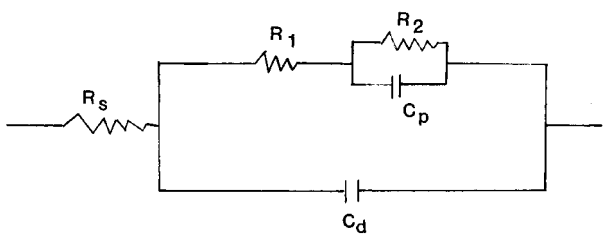

Fig. 6. Equivalent circuit of pyrite oxidation.

tion of the electric field on the electrode-solution interface [18]. To take into account the uneven distribution of the electric field, a resistance of a/ω, in parallel with the capacitance, was added to the equivalent circuit, where ω is the frequency and a is a constant depending on the characteristics of the electrode surface. Thus, the simplified equivalent circuit can be presented by the diagram shown in Figure 7.

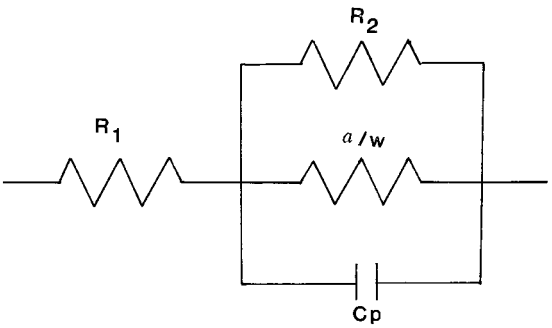

Fig. 7. Simplified equivalent circuit.

The impedance Z can be expressed as [19]

$$Z = Z' - jZ'' \tag{4}$$

where $j = (-1)^{1/2}$.

For the simplified equivalent circuit Z can be expressed as [20]

$$\begin{aligned} Z &= R_1 + \frac{1}{\left(\frac{1}{R_2} + \frac{\omega}{a}\right) + j\omega C_p} \\ &= R_1 + \frac{R_2 a(a + \omega R_2)}{(a + \omega R_2)^2 + (aR_2\omega C_p)^2} \\ &\quad - \frac{a^2 R_2^2 \omega C_p j}{(a + \omega R_2)^2 + (aR_2\omega C_p)^2} \end{aligned} \tag{5}$$

Thus, the real and the imaginary parts of the impedance are

$$Z' = R_1 + \frac{R_2 a(a + \omega R_2)}{(a + \omega R_2)^2 + (aR_2\omega C_p)^2} \tag{6}$$

and

$$Z'' = \frac{a^2 R_2^2 \omega C_p}{(a + \omega R_2)^2 + (aR_2\omega C_p)^2} \tag{7}$$

Since R_1 is the pivot of the depression of the semicircle in the complex plane plot, it can be neglected temporarily with $(R_1,0)$ as the new origin point and the impedance can be expressed in polar coordinates, as shown in Figure 8, where

$$\tan\theta = \frac{a^2 R_2^2 \omega C_p}{R_2 a(a + \omega R_2)} = \frac{aR_2\omega C_p}{a + \omega R_2} \tag{8}$$

$$\omega = \frac{1}{R_2}\tan\theta \Big/ \left(C_p - \frac{\tan\theta}{a}\right) \tag{9}$$

and

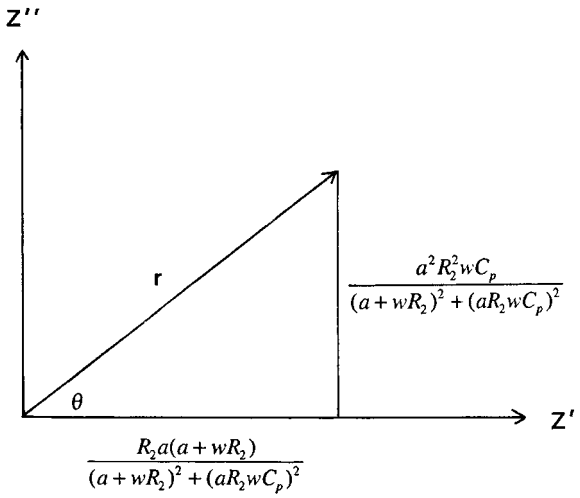

Fig. 8. Impedance expressed in polar coordinates.

$$\begin{aligned} r^2 &= \left(\frac{a^2 R_2^2 \omega C_p}{(a + \omega R_2)^2 + (aR_2\omega C_p)^2}\right)^2 \\ &\quad + \left(\frac{R_2 a(a + \omega R_2)}{(a + \omega R_2)^2 + (aR_2\omega C_p)^2}\right)^2 \\ &= \frac{a^2 R_2^2}{(a + \omega R_2)^2 + (aR_2\omega C_p)^2} \end{aligned} \tag{10}$$

It is obvious that, as shown in Figure 8,

$$r\sin\theta = \frac{a^2 R_2^2 \omega C_p}{(a + \omega R_2)^2 + (aR_2\omega C_p)} = r^2\omega C_p \tag{11}$$

and hence

$$r = \frac{\sin\theta}{\omega C_p} \tag{12}$$

By substituting Equation 9 into Equation 12, Equation 13 is obtained.

$$r = R_2\left(\cos\theta - \frac{1}{aC_p}\sin\theta\right) \tag{13}$$

Equation 15 is obtained if we let

$$\frac{1}{aC_p} = \tan\alpha \tag{14}$$

$$\begin{aligned} r &= R_2\left(\cos\theta\frac{\cos\alpha}{\cos\alpha} - \frac{\sin\alpha}{\cos\alpha}\sin\theta\right) \\ &= \frac{R_2}{\cos\alpha}\cos(\theta + \alpha) \end{aligned} \tag{15}$$

Equation 15 is an equation of the semicircle in polar coordinates with a depression angle of α against Z'-axis and $R_2/\cos\alpha$ is the diameter of the semicircle.

From equation 14, when $a = 0$, α is equal to $\pm\pi/2$. Since the complex plane plot was constructed on the first quadrant instead of the fourth quadrant by using $-Z''$ instead of Z'' (Figs 4 and 5), thus α was taken as 0. Then Equation 15 becomes

$$r = R_2 \cos\theta \tag{16}$$

Equation 16 represents a typical impedance semicircle without depression in polar coordinates. In Equation 15, $r = R_2$ when θ is equal to 0. Thus, R_2 is the intersection of the semicircle with the Z'-axis instead of the entire length of the diameter of the semicircle. When R_1 is taken into consideration, the intersections of the semicircle with the Z'-axis are R_1 and $R_1 + R_2$, respectively (Fig. 9).

The pseudo-capacitance, C_p, can be calculated through Equation 12, where the corresponding values of r and θ with respect to a particular ω can be obtained from the complex plot. The constant a can then be calculated according to Equation 14, where α is measured from the complex plane plot. The results for 1.10 V vs SHE are given in Table 1.

The double-layer capacitance per unit electrode area, C_d, is about $20\,\mu F\,cm^{-2}$ [21]. The resulting pseudo-capacitance, C_p, is $260\,\mu F\,cm^{-2}$ at 1.10 V, which is an order of magnitude greater than C_d. The assumption of the insignificance of C_d as compared to C_p, made in simplifying the equivalent circuit, is therefore valid. R_1 is equal to $10\ \Omega\,cm^2$ and $R_2 = 420 - 10 = 410\ \Omega\,cm^2$ (Fig. 5). The depression angle α was measured to be 29° and the constant a was calculated to be $6.9 \times 10^{-3}\,cm^2\,\mu F^{-1}$.

At 0.90 V, R_1 and R_2 were determined to be 12 and $480\ \Omega\,cm^2$, respectively. The depression angle was measured as 44°. The depression angle, as expressed in Equation 14, is a function of aC_p. The smaller depression angle at 1.10 V clearly is caused by the larger aC_p than that at 0.90 V.

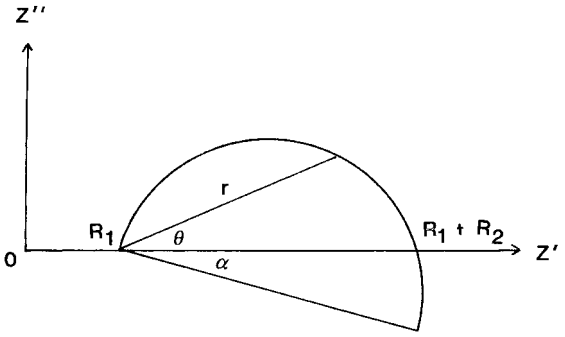

Fig. 9. Depressed semicircle with R_1 taken into consideration.

Table 1. Results obtained from complex plane plot at 1.10 V vs SHE

Points indicated in Fig. 4	ω /s^{-1}	θ /deg.	r /$\Omega\,cm^2$	C_p /$\mu F\,cm^{-2}$
1	5	22	301	2.49×10^2
2	7	27	256	2.53×10^2
3	10	34	214	2.61×10^2
4	15	40	168	2.55×10^2
5	20	45	135	2.66×10^2
6	30	50	96	2.65×10^2
7	40	52	75	2.62×10^2
8	60	55	53	2.57×10^2
9	90	60	38	2.53×10^2
10	120	63	29	2.56×10^2

Based on the simplified equivalent circuit shown in Figure 7, the peak charging current density at $t = 0^+$ for 1.10 V was calculated to be $i_c = E/R_1 = 110\,mA\,cm^{-2}$. At 0.90 V, the peak charging current density was found to be $75\,mA\,cm^{-2}$.

3.3. *Potential step chronoamperometric measurements*

While the kinetic parameters in the equivalent circuit, and hence the charging currents have been determined by the a.c. impedance measurements, it is desirable that the charging currents should be confirmed experimentally by another technique. The potential step chronoamperometric measurement was designed to do this.

In a potential step experiment, a potential pulse was applied to the electrode to transfer instantaneously the potential from an initial value where no faradaic current was flowing to an end potential where the surface concentration of the electrochemically active species was effectively zero. The duration of the final potential was controlled at 0.1 s. The results of the potential step measurement with the initial potential of 0.24 V and the final potential of 1.10 V are shown in Figure 10.

Both the charging and faradaic currents were clearly observed in Figure 10. During the initial 0.002 s, the charging current dominates and then the faradaic current becomes predominant when the capacitance is charged. At 1.10 V vs SHE, the faradaic current at $t = 0^+$ was determined to be 6 mA, using the method described by Lin and Zheng [17]. At 1.10 V, the observed peak current is 21 mA at $t = 0.001$ s. Thus the peak charging current is 15 mA and the peak charging current density is $105\,mA\,cm^{-2}$, which is comparable to the value of $110\,mA\,cm^{-2}$ obtained from the equivalent circuit coupled with the a.c. impedance measurements. In the potential step chronoamperometric measurement with

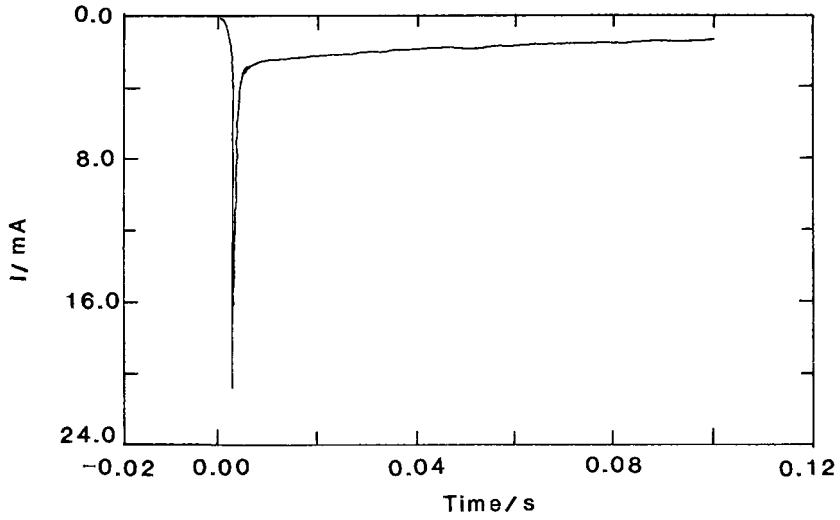

Fig. 10. Anodic current against transient time at 1.10 V in potential step measurement.

the end potential of 0.90 V, a peak charging current density of 69 mA cm^{-2} was obtained, which is comparable to that of the a.c. impedance measurement.

Pyrite is a well-known semiconductor with a band gap of about 0.9 eV. The semiconductor characteristic of pyrite is unlikely to have a significant impact on the a.c. impedance and the potential step chronoamperometric measurements when a relatively large potential is applied to the electrode.

4. Conclusions

Based on the cyclic voltammetric study, a two-step reaction model was proposed for the oxidation of pyrite. The first-step reaction involves the oxidation of pyrite to sulfur starting at 0.6 V. The second-step reaction is the oxidation of the sulfur to sulfate starting at 0.9 V. The peak shown in the voltammogram is caused by the passivation of the sulfur film, a product of the first reaction step. The reaction is controlled by the diffusion of ferric ions or electrons through the passivation film. This conclusion is consistent with the data plots of i_p against $v^{1/2}$ and i_p against disc rotating speed.

An equivalent circuit based on the oxidation reactions was postulated with the consideration of an uneven distribution of the electric field on the solution–electrode interface. The first-step and the second-step reaction resistances, and the pseudo-capacitance, as indicated in the equivalent circuit, have been determined to be 10 Ω cm^2, 410 Ω cm^2 and 260 μF cm^{-2}, respectively, at 1.10 V by the a.c. impedance measurements. At 0.90 V, the first-step and the second-step reaction resistances were determined to be 12 and 480 Ω cm^2, respectively.

In the a.c. impedance measurements, depressed semicircles were observed in the complex plane plots. A frequency-dependent resistance has been incorporated into the equivalent circuit and a mathematical formula has been derived to explain the depression of the semicircles. It is clearly demonstrated that the reaction resistance should be obtained from the intersection of the semicircle with the Z'-axis instead of the diameter when the semicircle is depressed. Reaction resistance, pseudo-capacitance, and depression angle of the semicircle have been obtained from the measurements and the mathematical formulas. The obtained pseudo-capacitance of 260 μF cm^{-2}, a magnitude greater than a typical electrical double-layer capacitance of 20 μF cm^{-2}, suggests that a passivation film forms on the surface of the electrode.

The equivalent circuit was then checked by using the potential step chronoamperometric technique. The peak charging current densities, which appear at $t = 0^+$, were calculated to be 110 and 75 mA cm^{-2} at 1.10 and 0.90 V, respectively, based on the proposed equivalent circuit and the a.c. impedance measurements. These current densities are comparable to the measured peak charging current densities of 105 and 69 mA cm^{-2} at 1.10 and 0.90 V, respectively, from the potential step chronoamperometric experiments.

Acknowledgements

The assistance of Z.M. Zheng, formerly with the Mineral Industry Research Laboratory, University of Alaska Fairbanks, is acknowledged.

References

1. R.T. Lowson, *Chem. Rev.* **82**(5) (1982) 461–97.
2. R.A. Meyers, *Coal Desulfurization*, Marcel Dekker, New York. (1977).
3. X. Zhu, J. Li, D.M. Bodily and M.E. Wadsworth, *J. Electrochem. Soc.* **140**(7) (1993) 1927–35.
4. X. Zhu, M.E. Wadsworth, D.M. Bodily and W.B. Hu, In: J.P. Hager (ed.) *A Comparative Study of the Electrochemical Properties of Mineral and Coal Pyrite*, EPD Congress, (1991) pp. 179–95.
5. S. Karth, R. Szargan and E. Suoninen, *Appl. Surf. Sci.* **72** (1993) 157–70.
6. E. Ahlberg, K.S.E. Forssberg and X. Wang, *J. Appl. Electrochem.* **20** (1990) 1033–39.
7. X. Zhu, J. Li and M.E. Wadsworth, *Colloids and Surfaces A: Physical and Engineering Aspects* **93** (1994) 201–10.
8. I.C. Hamilton and R. Woods, *J. Electoanal. Chem.* **118** (1981) 327–43.
9. S. Chander and A. Briceno, *Minerals Metal. Proc.* **8** (1987) 171–6.
10. N.D. Janetski, S.I. Woodburn and R. Woods, *Int. J. Mineral Proc.* **4** (1977) 227–39.
11. J. Li, X. Zhu and M.E. Wadsworth, In: J.P. Hager (ed.) *Raman Spectroscopy of Natural and Oxidized Metal Sulfides*, EPD Congress, (1993) 229–43.
12. F. Mansfeld, *Corrosion* **36**(5) (1981) 301–7.
13. D.C. Silverman, In: J.R. Scully (ed.) *Electrochemical Impedance: Analysis and Interpretation*, (1993) ASTM, Philadelphia, 192–204.
14. J. Pang, A. Briceno and S. Chander, *J. Electrochem. Soc.* **137**(11) (1990) 3447–55.
15. J. Pang and S.Chander, *Minerals Metal. Proc.* **9**(3) (1992) 131–6.
16. H.K. Lin and Z.M. Zheng, *Hydrometallurgy* **42** (1996) 411–24.
17. A.J. Bard and R.L. Faulkner, *Electrochemical Methods: Fundamentals and Application*, J. Wiley & Sons, New York (1980) pp. 213–48.
18. S. Iseki, K. Ohashi and S. Nagaura, *Electrochim. Acta* **17**(12) (1972) 2249–65.
19. D.D. MacDonald, *Transient Techniques in Electrochemistry*, Plenum Press, New York (1977) p. 267.
20. C.A. Desoer and E.S. Kuh, *Basic Circuit Theory*, McGraw-Hill, New York, (1969) pp. 289–99.
21. A.W. Adamson, *Physical Chemistry of Surfaces*, J. Wiley & Sons, New York (1967) p. 240.